Hindawi Publishing Corporation
Journal of Spectroscopy
Volume 2015, Article ID 126090, 11 pages
http://dx.doi.org/10.1155/2015/126090

Research Article

Canopy Spectral Characterization of Wheat Stripe Rust in Latent Period

Qi Liu, Yilin Gu, Shuhe Wang, Cuicui Wang, and Zhanhong Ma

Department of Plant Pathology, China Agricultural University, Beijing 100193, China

Correspondence should be addressed to Zhanhong Ma; mazh@cau.edu.cn

Received 29 June 2015; Revised 3 August 2015; Accepted 16 August 2015

Academic Editor: Daniel Cozzolino

Stripe rust, caused by *Puccinia striiformis* f. sp. *tritici* (*Pst*), is one of the important wheat diseases worldwide. In this study, the spectral data were collected from wheat canopy during the latent period inoculated with three different concentrations of urediniospores and classification models based on discriminant partial least squares (DPLS) were built to differentiate leaves with and without infection of the stripe rust pathogen. The effects of different spectra features, wavebands, and the number of the samples used in modeling on the performances of the models were assessed. The results showed that, in the spectral region of 325–1075 nm, the model with the spectral feature of 2nd derivative of Pseudoabsorption index had better accuracy than others. The average accuracy rate was 97.28% for the training set and 92.98% for the testing set. In the waveband of 925–1075 nm, the model with the spectral feature of 1st derivative Pseudoabsorption index had better accuracy than other models, and the average accuracy rates were 98.27% and 94.33% for the training and testing sets, respectively. The results demonstrated that wheat stripe rust in latent period can be qualitatively identified based on the canopy spectral detection. Thus, the method can be used for early monitoring of infections of wheat stripe rust.

1. Introduction

Wheat stripe rust, caused by *Puccinia striiformis* f. sp. *tritici* (*Pst*), is one of the most destructive diseases worldwide [1–5]. China is the largest wheat-producing and consuming country in the world, where stripe rust has caused heavy yield losses. For example, in 1950, 1964, 1990, and 2002, stripe rust caused yield losses up to 6.0, 3.0, 1.8, and 1.3 million metric tons, respectively [6–8]. During pandemics of wheat stripe rust in China, urediniospores of the pathogen can be transported over a long distance across different geographic regions, and the pathogen requires special climates for its overwintering and oversummering [9]. As an obligate parasite [10–12], *Pst* should overwinter and oversummer in living wheat plants to complete its life cycle [13]. The whole infection process by *Pst* can be divided into four periods, that is, the contact period, the invasion period, the latent period, and the diseased period. In the latent period, the pathogen spreads within host tissues although people cannot see this process with the naked eye. At the early stage of latent infection, the pathogen would consume the nutrients and moisturein host to grow and extend, which resulted in multifaceted changes in the metabolism of the wheat, the cell content, the color pigments, and the moisture content, and the cell gaps were affected significantly [14]. In the late stage of latent period, the chlorosis spots are the typical symptom on the leaves. Once the condition is suitable for development of the disease, the disease would appear. Accurate disease diagnoses, rapid detection, and identification of plant pathogens were of utmost importance for controlling plant diseases and mitigating the economic losses that incur. However, the most widely used method for detecting wheat stripe rust was visual survey which was labor costing, time consuming, and subjective. Furthermore, by the time visual and tactile signs were evident, yield-limiting damage might have already occurred. Therefore, it is necessary to develop a new method to identify and assess this disease, especially during the latent period. Efficient detection and estimation of latent infections in leaves could provide critical information for disease prediction. The pathogen in latent infection of wheat leaves usually serves as inoculum of epidemics. Detection of initial inoculums in early growing season is important in disease prediction and management.

Nowadays, wheat stripe rust is the major obstacle to stable and high yield of wheat [15, 16]. Monitoring and early detection of this disease is crucial for the effective control and implementation of measures. Recent developments of remote sensing technology had the potential to enable direct detection of plant diseases under field conditions [17–19]. Moreover, spectral remote sensing had been paid great attention to and had been applied successfully to monitor stripe rust at different platforms, such as the single leaf platform [20–22], the ground remote sensing platform [23–25], the airborne remote sensing platform [26–28], and the space remote sensing platform [29–31]. Previous research showed that it was simple to distinguish the objects from each other because each object has its special reflectance property. Taking healthy plants as an example, the leaf reflectance was low in the blue (about 0.45 to 0.52 μm), peaks in the green (about 0.52 to 0.55 μm), and decreases to a minimum in the red (about 0.63 to 0.70 μm) regions. The low reflectance in the blue and red regions was generally attributed to absorption by chlorophyll. Gates et al. [32] stated that chlorophyll, carotenes, and xanthophylls absorb radiation at 0.445 μm, but only chlorophyll absorbs in the red region (near 0.645 μm). Thus, healthy green leaves exhibited low reflectance values in the blue and red portions of the spectrum, and an increase in reflectance in these wavebands might signal a stress condition. The green peak accounts for the green color of plants perceived by the human eyes. The high reflectance of leaves in the near-infrared region (about 0.7 to 1.3 μm) was apparently caused by their internal cellular structure [33]. Radiation was diffused and scattered through the cuticle and epidermis to the mesophyll cells and air cavities in the interior of the leaf. Radiation was further scattered by multiple reflections and refractions at the interface of hydrated cell walls with intercellular air spaces because of refractive index differences (1.4 for hydrated cells and 1.0 for air). 40% to 60% of the incident near-infrared radiation was scattered upward through the surface of incidence and was designated as reflected radiation, whereas the remainder was scattered downward and was designated as transmitted radiation, and little radiation, if any, was absorbed. This phenomenon has been extensively studied [34–36]. Physiological and anatomical changes are caused within plants as a result of stress. Plant pathogens may change leaf color by causing chemical changes within plant cells or by growing on plant surfaces [37]. So, in the latent period of wheat stripe rust, the most obvious color change was the chlorosis spots on the leaves.

In this study, the potential usefulness of an ASD spectroradiometer to detect wheat stripe rust in the latent period was investigated. The canopy spectral data were collected and the models were evaluated by using the method of DPLS. The objective of this study was to use the canopy spectral data of wheat stripe rust in the latent period to provide a method for early monitoring and evaluating this disease.

2. Materials and Methods

2.1. Experimental Material. All experimental materials were prepared in the Lab of Plant Disease Epidemiology, Department of Plant Pathology, China Agricultural University, in 2013. Mingxian 169, a wheat variety which is highly susceptible to *Pst*, was used in the study. The seeds of Mingxian 169 were soaked for 24 h in sterile water and then sowed in pots (10 cm in diameter) at a density of approximately 25 seeds per pot, 40 pots totally. Then, the potted plants were grown in the artificial climate chamber at 11~13°C with 60~70% relative humidity (RH) and 12 h of light per day (10,000 lux). When the first leaves of wheat seedlings were fully expanded, the plants were sprayed with urediniospores of three predominant races of *Pst*, CYR31 (China Yellow Race 31), CYR32, and CYR33, at concentrations of 0.2 (number 1), 0.1 (number 2), and 0.05 (number 3) mg/mL. Spore suspension of each concentration was sprayed on plants for ten pots as treatment groups, and the remaining ten pots were sprayed by distilled water as healthy control group. Immediately after inoculation, the wheat seedlings were transferred into a moist chamber under dark conditions at 11~13°C for 24 h. Then, the wheat seedlings were sealed with transparent plastic and incubated in the artificial climate chamber. After 12 days of incubation, uredinia appeared on all the treatment groups' leaves and this indicated that the inoculation experiment was successful, so the latent period of wheat stripe rust was 11 days. During the whole latent period, the spectral data was obtained on the day before inoculation and on the 3rd, 6th, 9th, and 10th day after inoculation.

2.2. Acquisition of Spectral Data. An ASD spectroradiometer (ASD FieldSpec HandHeld 2) (ASD Inc., Boulder, Colorado, USA) was used to collect the canopy spectral data of wheat. It is a portable spectroradiometer that performs rapid, precise, nondestructive, and noncontact measurements. The HandHeld 2 employs a unique spectrometer operating in a range of 325–1075 nm, a wavelength accuracy of ±1 nm, a spectral resolution of <3 nm at 700 nm, 25° field of view, and minimum integration time of 8.5 ms, which produces high signal-to-noise ratio spectra in under a second using a highly sensitive detector array, low stray light grating, built-in shutter, Drift-Lock dark current compensation, and second-order filtering. The HandHeld 2 provides extremely accurate, quickly derived reflectance, radiance, and irradiance spectra in a variety of settings. The measurements were conducted on clear, sunny days from 10:00 am to 2:00 pm. Before each measurement, a white reference panel was taken to optimize the instrument. When the baseline was nearly 100% (reflectance values of 1 at each wavelength), the measurements were carried on. The spectrum average set value was 15. Three spectra were measured for each pot, and the average value was treated as the canopy spectrum at the point. The spectroradiometer, facing the center of the pot, was positioned vertically to the wheat canopy at a height of 0.2 m above with a view area of about 0.00785 m^2 (according to ASD sampling surface and the distance formula, the sampling vertical distance was set at 20 cm which was suitable for the 10 cm diameter pots under the outdoor conditions with sunlight as the light source). A total of 600 reflectance spectra were used for subsequent analysis. The spectra included 120 canopy spectra of healthy wheat (control group before inoculation), 120 canopy spectra

of healthy wheat in the same growth period, and 360 canopy spectra of treatment group in the latent period.

2.3. Preprocessing of Spectral Data. Derivative transform is one of the most commonly used methods for spectral preprocessing, in which the background interference and the atmospheric scattering effect can be reduced or eliminated and the contrast of the different absorption characteristics improved. The first derivative transform can partially eliminate the linear and quadratic background noise; the second derivative spectra can completely eliminate the effects of linear background noise and can basically eliminate quadratic background noise. In the analysis of vegetation canopy spectra, the application of derivative transformation has also been very popular. The use of derivative spectra is an established technique in analytical chemistry for the elimination of background signals and for resolving overlapping spectral features. Application of this technique for tackling analogous problems such as interference from soil background reflectance in the remote sensing of vegetation or for resolving complex spectra of several target species within individual pixels in remote sensing is proposed. And the use of derivatives for monitoring chlorosis in vegetation shows that derivative spectral indices are superior to conventional broadband spectral indices such as the near-infrared/red reflectance ratio [38]. The canopy spectra of wheat, the spectra of soil background, and the spectra of the first derivative values' difference were compared, and the results indicated that the derivative transform can easily confirm the bending point of spectral curve, the positions of the maximum and minimum wavelength. In the variation of the spectrum, such as the blue edge, yellow edge, and red edge of the vegetation spectrum, the derivative transform can eliminate the interference of soil background. Derivative spectra are very sensitive on the spectral signal-to-noise ratio [39]. Therefore, some other methods had been derived from the derivative spectrum, such as high-order derivative method, logarithmic derivative method, and high-order logarithmic derivative method. The logarithmic derivative method generally refers to the logarithm of the reflectance (log R) or the logarithm of reflectance reciprocal [log(1/R)]. log(1/R), defined as pseudoabsorption index, can reflect the absorption characteristics of objects. Due to the lower vegetation spectral reflectance in the visible region, logarithmic derivative method is necessary which can not only enhance the spectral differences in visible region, but also reduce multiplicative factors effect caused by the changes of illumination [40–44]. Based on the previous research, using the software of ViewSpecPro provided by ASD, in this study, six variables were derived for modeling including the original spectrum reflectance (R), the first derivative of reflectance (R_1st.dv), the second derivative of reflectance (R_2nd.dv), the pseudoabsorption index or the logarithm of R or 1/R[log(1/R)], the first derivative of log(1/R)[log(1/R)_1st.dv], and the second derivative of log(1/R)[log(1/R)_2nd.dv].

The qualitative partial least squares regression (discriminant partial least squares, DPLS) of MATLAB R2010a software was used for processing the spectral data. PLS provides a multiple linear regression modeling method, especially for data containing a lot of correlated variables but few observations; the PLS model performs better than the other traditional regression analysis methods. The PLS method combines the advantages of the principal component analysis (PCA), canonical correlation analysis (CCA), and linear regression analysis method, so it can result in a more reasonable and more comprehensive regression model. Based on PLS, the DPLS uses linear regression to analyze the spectral data with the categorical variables. First, the discrimination process needs to identify the classification variables from calibration samples. Then, the PLS model between spectral data and categorical variables was obtained. According to the calibration set of the PLS model, from classification variables and spectral characteristics, the samples of the testing set were verified later [45]. The DPLS method's discriminability was highly efficient because the auxiliary matrices' class information with the form of code was taken into account. At the same time, the principal component extracted not only was most related to the category, but also had good analytical ability on the categories information matrix. So the sample spectrums' scores of these components can be used as spectral characteristics, and the principal components had a much smaller dimension than the original sample spectra. Therefore, the DPLS characteristics extraction method also had a dimension reduction effect [46].

3. Results

3.1. The Spectral Curves of Different Concentrations and Different Times. Figures 1(a), 1(b), and 1(c) showed the wheat canopy spectral changes of three different inoculation concentrations on the 1st day before inoculation and on the 3rd day, 6th day, 9th day, and 10th day after inoculation. Each spectrum was derived from the average spectrum of the treatment group at different inoculum concentrations. According to Figure 1, the variation trend of the wheat canopy spectra at number 1 inoculum concentration was basically consistent with number 2 inoculum concentration: during the latent period of 1–9 days, the reflectivity of 400~700 nm increased along with the time increase and reached the maximum on the 9th day. The green peak near the 550 nm and the red valley near the 670 nm changed obviously. Since the 670 nm band is the absorption band of chlorophyll, the increase of the green peak and decrease of the red valley indicated that the chlorophyll content of wheat leaves decreased continuously over time. The 700~780 nm band, known as the "red edge" of the vegetation reflectance, shifted to the blue band with the latent time increase, indicating that the wheat growth was influenced by the *Pst* infection to some extent; the 780~1050 nm band mainly reflects the leaves internal structure characteristics. The reflectance increased with the latent period of wheat stripe rust and reached the highest value on the 9th day. This phenomenon indicated that the internal structure of wheat leaves would change by the *Pst* infection, and then the spectral reflectance was further affected. On the 10th day of the latent period, the spectral reflectance of all bands decreased to some extent and the reflectance of the 780~1050 nm band decreased greatly. The whole spectral curve on the 10th day was similar to the

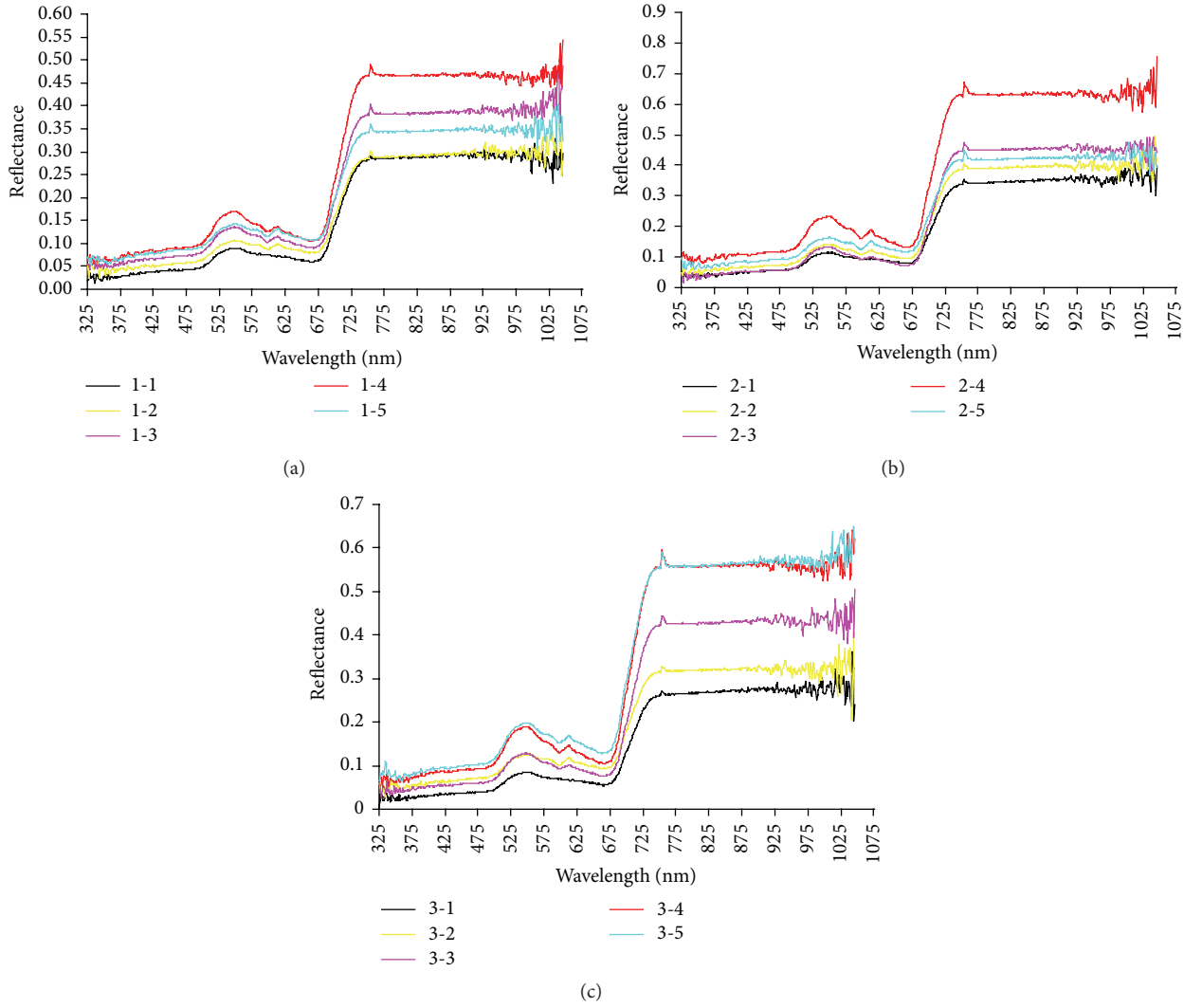

Figure 1: Wheat leaf canopy spectra curves of 1st (a), 2nd (b), and 3rd (c) inoculation concentrations.

spectral curve on the 6th day. The canopy spectral variation of number 3 *Pst* concentration in the latent period of the former nine days was the same as those of number 1 and number 2 *Pst* concentrations, but the spectral reflectance of each band on the 10th day has not significantly changed from the 9th day. Because the high inoculation concentration caused high primary infection quantity and number 3 concentration was lower than number 1 and number 2 concentrations in this study, the results may infer the following: The changes of the wheat canopy spectra were not correlated with the inoculation concentration in the latent period of the former nine days but were mainly caused by the wheat defense response, and this process of reaction was only connected with the infection of *Pst* but not the infection quantity; with the development of this disease, the *Pst* content in the wheat leaves has become the main reason for the spectral changes, including the pathogen and its metabolites amount increasing. Therefore, with the comprehensive effects of *Pst* and its variation in wheat, the canopy spectral reflectance showed a decrease trend, and the decreased degree was related to the initial inoculation concentration on the 10th day of latent period.

3.2. Prediction Results of Different Models with Different Spectral Features on the 325–1075 nm. For deep mining the spectral information, different models were proposed according to the number of samples and spectral features by the DPLS method on the 325–1075 nm band (Tables 1–6). To use the reflectivity as spectral feature of modeling in the 325–1075 nm band, the average accuracy was 97.12% for the training set and 85.13% for the testing set (Table 1). When the ratio of training set to testing set was 4 : 1, the model had better recognition than the other models, four principal components were included, and the accuracy was 96.67% and 90.00% for the training and testing sets, respectively. To use *R*_1st.dv as spectral feature of modeling in the 325–1075 nm band, the average accuracy was 99.03% for the training set and 79.10% for testing set (Table 2). When the ratio of training set and testing set was 1 : 1, the model had better recognition effect than the other models, three principal components

Table 1: Prediction accuracy of models resulting from different ratios of training set to testing set based on reflectance.

Modeling ratio		Accuracy	
(TrS : TeS)	PCN	TrSA%	TeSA%
1 : 1	4	97.33	84.00
2 : 1	4	98.00	78.00
3 : 1	4	96.46	89.19
4 : 1	4	96.67	90.00
Mean	4	97.12	85.30

Table 2: Prediction accuracy of models resulting from different ratios of training set to testing set based on 1st derivative of reflectance.

Modeling ratio		Accuracy	
(TrS : TeS)	PCN	TrSA%	TeSA%
1 : 1	3	98.67	80.00
2 : 1	3	100	78.00
3 : 1	3	99.12	78.38
4 : 1	3	98.33	80.00
Mean	3	99.03	79.10

Table 3: Prediction accuracy of models resulting from different ratios of training set to testing set based on 2nd derivative of reflectance.

Modeling ratio		Accuracy	
(TrS : TeS)	PCN	TrSA%	TeSA%
1 : 1	3	97.33	78.67
2 : 1	3	98.00	76.00
3 : 1	4	95.58	89.19
4 : 1	4	96.67	93.33
Mean	3.5	96.90	84.30

Table 4: Prediction accuracy of models resulting from different ratios of training set to testing set based on $\log(1/R)$.

Modeling ratio		Accuracy	
(TrS : TeS)	PCN	TrSA%	TeSA%
1 : 1	8	100	83.67
2 : 1	8	98.00	74.00
3 : 1	7	95.58	83.73
4 : 1	10	97.50	96.67
Mean	8.25	97.77	84.52

were included, and the accuracy was 98.67% and 80.00% for the training and testing sets, respectively. To use R_2nd.dv as spectral feature of modeling in the 325–1075 nm band, the average accuracy was 96.90% for the training set and 84.30% for the testing set (Table 3). When the ratio of training set and testing set was 4 : 1, the model had better recognition than the other models, four principal components were included, and the accuracy was 96.67% and 93.33% for the training and testing sets, respectively. To use $\log(1/R)$ as spectral feature of modeling in the 325–1075 nm band, the average accuracy was 97.77% for the training set and 84.52% for the testing set (Table 4). And when the ratio of training set and testing set was 4 : 1, the model had better recognition than the other models, ten principal components were included, and the accuracy was 97.50% and 96.67% for the training and testing sets, respectively. To use $\log(1/R)$_1st.dv as spectral feature of modeling in the 325–1075 nm band, the average accuracy was 98.14% for the training set and 91.15% for the testing set (Table 5). When the ratio of training set and testing set was 3 : 1, the model had better recognition than the other models, eight principal components were included, and the accuracy was 98.23% and 94.59% for the training and testing sets, respectively. To use $\log(1/R)$_2nd.dv as spectral feature of modeling in the 325–1075 nm band, the average accuracy was 97.89% for the training set and 92.98% for the testing set (Table 6). When the ratio of training set and testing set was 3 : 1, the model had better recognition than the other models, eight principal components were included, and the accuracy was 98.23% and 94.59% for the training and testing sets, respectively. In conclusion, the models with $\log(1/R)$_2nd.dv showed the best accuracy so that $\log(1/R)$_2nd.dv should be taken as the priority parameter for modeling.

Table 5: Prediction accuracy of models resulting from different ratios of training set to testing set based on $\log(1/R)$'s 1st derivative.

Modeling ratio		Accuracy	
(TrS : TeS)	PCN	TrSA%	TeSA%
1 : 1	7	98.67	92.00
2 : 1	9	99.00	88.00
3 : 1	8	98.23	94.59
4 : 1	10	96.67	90.00
Mean	8.5	98.14	91.15

Table 6: Prediction accuracy of models resulting from different ratios of training set to testing set based on $\log(1/R)$'s 2nd derivative.

Modeling ratio		Accuracy	
(TrS : TeS)	PCN	TrSA%	TeSA%
1 : 1	7	96.00	93.33
2 : 1	10	99.00	94.00
3 : 1	8	98.23	94.59
4 : 1	11	98.33	90.00
Mean	9	97.89	92.98

3.3. Discrimination Accuracy of Different Models with Different Spectral Features on Different Wavelengths. The method with different spectral features in the wavelength of 325–1075 nm needed more calculation, ran slower, analyzed a wider spectral region, and had more invalid information and lower effective information, so the spectral identification rate could not reach the highest value. In addition, if the selection of spectral region was too narrow, it may omit effective information and lower the identification accuracy of the model. To find the more effective information band, modeling was processed with five wavelengths (325–474 nm, 475–624 nm, 625–774 nm, 775–924 nm, and 925–1075 nm) in 325–1075 nm spectral region according to the different

Table 7: Prediction results of different sampling model built in 325–474 nm.

Spectra features	Modeling ratio				
	1 : 1	2 : 1	3 : 1	4 : 1	Mean
R					
PCN	3	4	3	4	3.5
TrSA%	96.00	97.00	95.58	97.50	96.52
TeSA%	76.00	90.00	81.08	93.33	85.10
R_1st.dv					
PCN	4	3	4	3	3.5
TrSA%	94.67	98.00	96.46	95.83	96.24
TeSA%	96.00	80.00	89.19	66.67	82.96
R_2nd.dv					
PCN	7	7	6	6	6.5
TrSA%	98.67	98.00	96.46	95.83	97.24
TeSA%	94.67	94.00	94.59	90.00	93.32
log(1/R)					
PCN	7	7	7	8	7.25
TrSA%	98.67	97.00	97.35	96.67	97.42
TeSA%	97.33	92.00	94.59	90.00	93.48
log(1/R)_1st.dv					
PCN	9	10	8	11	9.5
TrSA%	97.33	96	95.58	95.83	96.19
TeSA%	90.67	94.00	83.78	86.67	88.78
log(1/R)_2nd.dv					
PCN	9	11	9	13	10.5
TrSA%	96.00	96.00	95.58	97.50	96.27
TeSA%	81.33	94.00	86.49	93.33	88.79

Table 8: Prediction results of different sampling model built in 475–624 nm.

Spectra features	Modeling ratio				
	1 : 1	2 : 1	3 : 1	4 : 1	Mean
R					
PCN	6	6	6	6	6
TrSA%	98.67	98.00	97.35	97.5	97.88
TeSA%	81.33	90.00	81.08	83.33	83.94
R_1st.dv					
PCN	4	4	4	5	4.25
TrSA%	97.33	96	96.46	98.33	97.03
TeSA%	76	82	81.08	96.67	83.94
R_2nd.dv					
PCN	3	5	3	4	3.75
TrSA%	96.00	98.00	95.58	95.83	96.35
TeSA%	74.67	96.00	75.68	96.67	85.76
log(1/R)					
PCN	6	6	6	6	6
TrSA%	96.00	98.00	95.58	96.67	96.56
TeSA%	86.67	84.00	89.19	86.67	86.63
log(1/R)_1st.dv					
PCN	5	5	5	5	5
TrSA%	98.67	100	100	98.33	99.25
TeSA%	85.33	94.00	91.89	86.67	89.47
log(1/R)_2nd.dv					
PCN	3	3	3	3	3
TrSA%	98.67	96.00	95.58	98.33	97.15
TeSA%	73.33	76.00	81.08	80	77.60

spectral modeling features. The results were shown in Tables 7–11.

As shown in Figures 2(a) and 2(b), the average accuracy of different models differed little for the training sets but varied largely for the testing sets. The models with log(1/R)_1st.dv or log(1/R)_2nd.dv as spectral feature in the 325–1075 nm band were better than the other models, and the average accuracy was over 98.00% for the training set and higher than 90.00% for the testing set. When using R_1st.dv as modeling spectrum feature, the average accuracy was 99.03% and 79.1% for the training and testing sets, respectively, suggesting that this model had good abilities in self-learning and predicting, but the generalization error was relatively large. Selecting 325–474 nm as modeling waveband, the models with log(1/R) and reflectance as spectra features' accuracy were better than others, the former's average accuracy was 97.42% and 93.48% for the training and testing sets, respectively, and the latter's average accuracy was 97.24% and 93.32% for the training and testing sets, respectively; the testing set average accuracies of other models were all below 90%. Selecting 475–624 nm as modeling waveband, the model with log(1/R)_1st.dv as spectrum feature's accuracy was better than others, and the average accuracy was 99.25% and 89.47% for the training and testing sets, respectively; selecting 625–474 nm as modeling waveband, the models with log(1/R)_2nd.dv and reflectance as spectra features' accuracy were better than others, the former's average accuracy was 97.80% and 92.31% for the training and testing sets, respectively, and the latter's average accuracy was 97.89% and 92.14% for the training and testing sets, respectively. Selecting 775–924 nm as modeling waveband, the models with reflectance and R_1st.dv as spectra features' accuracy were better than others, the former's average accuracy was 97.93% and 91.48% for the training and testing sets, respectively, and the latter's average accuracy was 97.75% and 92.30% for the training and testing sets, respectively; selecting 925–1075 nm as modeling waveband, the models with log(1/R) and log(1/R)_1st.dv as spectra features' accuracy were better than others, the former's average accuracies were 98.43% and 92.47% for the training set and the testing set, respectively, and the latter's average accuracies were 98.27% and 94.33% for the training set and the testing set, respectively.

As shown in Figures 3(a) and 3(b), selecting original spectrum as modeling spectrum feature, the models on the 625–774 nm and 775–924 nm wavebands accuracy were better than others, the former's average accuracy was 97.80% and 92.31% for the training and testing sets, respectively, and the latter's average accuracies were 97.93% and 91.48% for the training set and the testing set, respectively. Selecting R_1st.dv as modeling spectrum feature, the models on the 775–924 nm waveband accuracy were better than others, and the average accuracies were 97.75% and 92.30% for the training set and

Table 9: Prediction results of different sampling model built in 625–774 nm.

Spectra features	Modeling ratio				
	1 : 1	2 : 1	3 : 1	4 : 1	Mean
R					
PCN	6	7	7	6	6.5
TrSA%	97.33	99.00	97.35	97.50	97.80
TeSA%	93.33	94.00	91.89	90.00	92.31
R_1st.dv					
PCN	5	5	6	5	5.25
TrSA%	96.00	96.00	97.35	95.83	96.30
TeSA%	84.00	88.00	94.59	86.67	88.32
R_2nd.dv					
PCN	5	5	5	4	4.75
TrSA%	97.33	96.00	97.35	95.83	96.63
TeSA%	92.00	92.00	91.89	83.33	89.81
log(1/R)					
PCN	6	6	7	7	6.5
TrSA%	96.00	96.00	99.12	98.33	97.36
TeSA%	84.00	86.00	97.30	90.00	89.33
log(1/R)_1st.dv					
PCN	5	5	5	5	5
TrSA%	97.33	99.00	98.23	98.33	98.22
TeSA%	92.00	86.00	91.89	90.00	89.97
log(1/R)_2nd.dv					
PCN	5	5	5	4	4.75
TrSA%	98.67	98.00	98.23	96.67	97.89
TeSA%	93.33	90.00	91.89	93.33	92.14

Table 10: Prediction results of different sampling model built in 775–924 nm.

Spectra features	Modeling ratio				
	1 : 1	2 : 1	3 : 1	4 : 1	Mean
R					
PCN	4	5	5	5	4.75
TrSA%	97.33	97.00	98.23	99.17	97.93
TeSA%	82.67	92.00	94.59	96.67	91.48
R_1st.dv					
PCN	4	5	5	5	4.75
TrSA%	97.33	98.00	97.35	98.33	97.75
TeSA%	94.67	92.00	89.19	93.33	92.30
R_2nd.dv					
PCN	5	5	5	6	5.25
TrSA%	96.00	96.00	95.58	97.50	96.27
TeSA%	92.00	92.00	89.19	90.00	90.80
log(1/R)					
PCN	4	5	5	5	4.75
TrSA%	96.00	97.00	99.12	97.50	97.41
TeSA%	78.67	90.00	89.19	90.00	86.97
log(1/R)_1st.dv					
PCN	3	5	4	3	3.75
TrSA%	98.67	97.00	95.58	95.83	96.77
TeSA%	77.33	100	89.19	76.67	85.80
log(1/R)_2nd.dv					
PCN	4	4	5	5	4.5
TrSA%	96.00	96.00	95.58	95.83	95.85
TeSA%	82.67	96.00	86.49	93.33	89.62

the testing set, respectively. Selecting R_2nd.dv as modeling spectrum feature, the models on the 325–474 nm and 775–924 nm wavebands accuracy were better than others, and the former's average accuracies were 97.24% and 93.32% for the training set and the testing set, respectively, and the latter's average accuracies were 96.27% and 90.80% for the training set and the testing set, respectively. Selecting log(1/R) as modeling spectrum feature, the models on the 325–474 nm and 925–1075 nm wavebands accuracy were better than others, and the former's average accuracies were 97.42% and 93.48% for the training set and the testing set, respectively, and the latter's average accuracies were 98.43% and 92.47% for the training set and the testing set, respectively. Selecting log(1/R)_1st.dv as modeling spectrum feature, the models on the 325–1075 nm and 925–1075 nm wavebands accuracy were better than others, and the former's average accuracies were 98.14% and 91.15% for the training set and the testing set, respectively, and the latter's average accuracies were 98.27% and 94.33% for the training and testing sets, respectively. Selecting log(1/R)_2nd.dv as modeling spectrum feature, the models on the 325–1075 nm, 625–774 nm, and 925–1075 nm wavebands accuracy were better than others, the average accuracies for training sets were 97.89%, 97.89%, and 96.31%, respectively, and the average accuracies for testing sets were 92.98%, 92.14%, and 93.65%, respectively.

In conclusion, the model selected log(1/R)_1st.dv and 925–1075 nm waveband as spectral features, and the average accuracies were 98.27% and 94.33% for the training and testing sets, respectively. Different wavebands reflected different information of the plant and different spectra features transform increased the information mining from different perspective. Therefore, to establish the models which had higher accuracy rate, increased robustness, and generalization ability, in the future studies, it is necessary to build a variety of models which have different wavebands and different spectral transformations of original spectra. Combining all the model's predictions, the testing sample categories were decided by vote.

4. Discussion and Conclusions

This study was still at the exploratory stage. Reports on remote sensing in monitoring wheat stripe rust were few, and previous studies mainly focused on spectrum properties of rice blast or wheat powdery mildew, or the spectrum curve's similarities and differences between diseased crops and healthy crops. In this study, an ASD FieldSpec spectrometer was used to study the canopy spectral properties of wheat in the latent period infected by *Pst*. Models with different *Pst* concentrations, modeling proportion, spectra features, and wavebands were assessed using DPLS, a practical, robust,

Table 11: Prediction results of different sampling model built in 925–1075 nm.

Spectra features	Modeling ratio				
	1 : 1	2 : 1	3 : 1	4 : 1	Mean
R					
PCN	3	3	3	3	3
TrSA%	97.33	97.00	96.46	96.67	96.87
TeSA%	72.00	72.00	78.38	73.33	73.93
R_1st.dv					
PCN	3	3	3	3	3
TrSA%	97.33	100	97.35	97.50	98.05
TeSA%	80.00	80.00	81.08	76.67	79.44
R_2nd.dv					
PCN	3	3	4	4	3.5
TrSA%	97.33	98.00	95.58	95.83	96.69
TeSA%	78.67	76.00	89.19	93.33	84.30
log(1/R)					
PCN	5	8	6	7	6.5
TrSA%	100	98.00	98.23	97.50	98.43
TeSA%	85.33	96.00	91.89	96.67	92.47
log(1/R)_1st.dv					
PCN	7	8	7	8	7.5
TrSA%	98.67	97.00	98.23	99.17	98.27
TeSA%	94.67	92.00	97.30	93.33	94.33
log(1/R)_2nd.dv					
PCN	7	8	7	9	7.75
TrSA%	96.00	97.00	95.58	96.67	96.31
TeSA%	94.67	92.00	94.59	93.33	93.65

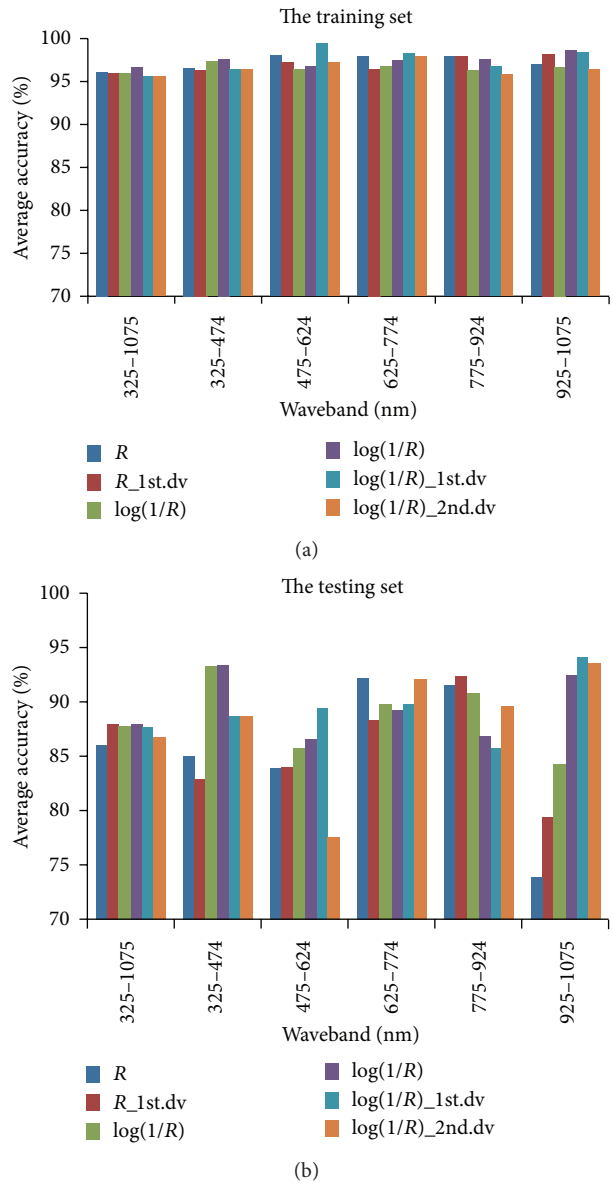

Figure 2: (a) The training sets average accuracy of different sampling model based on different spectra features and the same waveband. (b) The testing sets average accuracy of different sampling model based on different spectra features and the same waveband.

readily available, and cost-effective method. The results showed that the model which selected log(1/R)_2nd.dv as modeling spectrum feature in the 325–1074 nm waveband was better than the other models. Meanwhile, different modeling proportions also affected the accuracy of the models, and a modeling ratio of 4 : 1 (training set : testing set) resulted in better accuracy than the other ratios. The waveband selection was also very important for modeling: selecting narrow wavebands, the effective information may be missed; selecting wide wavebands, the invalid information may be too much and the modeling has lower efficiency. With the same modeling proportion and spectra features, there always existed a model with subband which had a better-than-average accuracy for its testing set. The results showed that the models with better accuracy were mainly focused on the 625–1075 nm waveband. This was consistent with the previous studies and in good agreement with the physiological change of wheat stressed by *Pst*. With the infection of *Pst*, the foliar superficial structure and the mesophyll cells of wheat were destroyed, which caused the leaf water content and the chlorophyll content to take a downward trend. The leaf internal structure was also changed with the accumulation of *Pst*. In the latent period, the most obvious symptom of the wheat leaves was chlorosis spots and yellow discoloration. Because the 460–680 nm waveband was related to the vegetation pigment content and the 750–1300 nm waveband was correlated with vegetation water content, the canopy spectral reflectance changed more obviously [47]. The models in this study had a good recognition effect, in which the wavebands mainly focused on the 625–1075 nm.

Spectral remote sensing is a breakthrough technology which can obtain relevant spectral data of the interesting objects from many narrow defined channels [48]. As the spectral remote sensing data could provide ample property information of the objects on the earth, the spectral information of target objects could be studied in the nm level wavelength band. Therefore, the spectral information of continuum wavelength band which traditional remote sensing cannot provide could be obtained now. The final

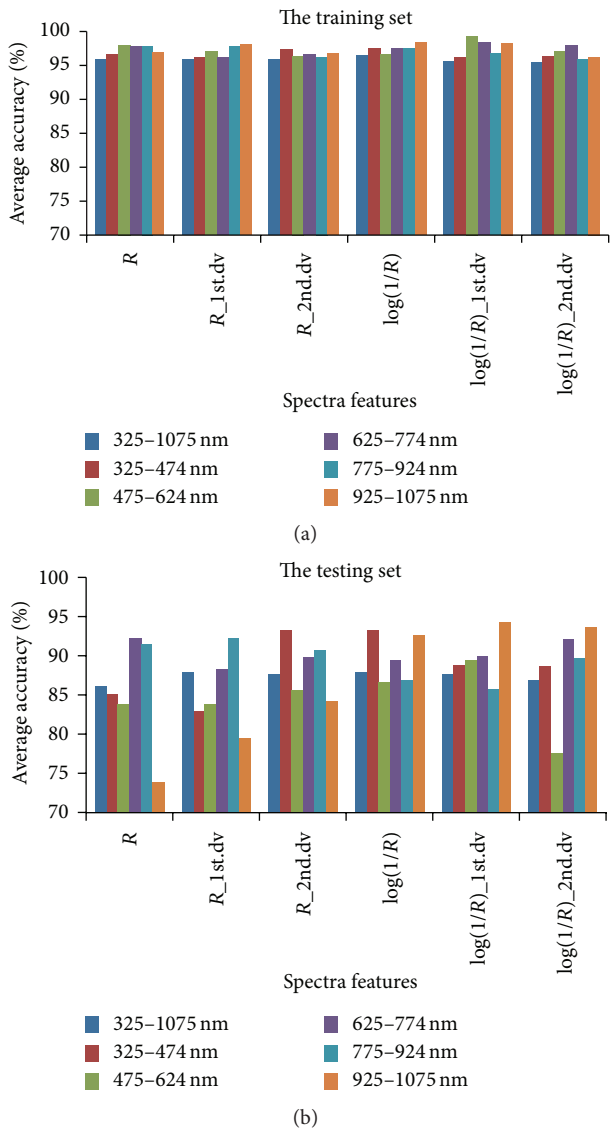

Figure 3: (a) The training sets average accuracy of different sampling model based on different wavebands and the same spectra features. (b) The testing sets average accuracy of different sampling model based on different wavebands and the same spectra features.

objective of this study was to detect the infections of stripe rust at latent period with DPLS, and the information can be used to estimate possible infection levels before disease appearance. Such estimated infection level serves as a reference of inocula, initiating disease epidemics in the coming season. All materials of this study were obtained from the artificial climate chamber which was not affected by the external environment, so the models' accuracy was relatively high. However, wheat in the field environment was more complex and affected by various interference factors. The use of spectral remote sensing technology for monitoring wheat stripe rust in the field will be the next research focus. The potential applications of this method will be in rapid and precise decision-making on disease management early in the season.

Abbreviations

PLS:	Partial least squares regression
DPLS:	Discriminant partial least squares
PCA:	Principal component analysis
PCN:	Principal component number
TrSA:	Training set accuracy
TeSA:	Testing set accuracy
CYR:	China Yellow Race
Pst:	*Puccinia striiformis* f. sp. *tritici*
R:	Reflectance
*R*_1st.dv:	The first derivative of reflectance
*R*_2nd.dv:	The second derivative of reflectance
log(1/*R*):	Pseudoabsorption index/the logarithm of *R* or 1/*R*
log(1/*R*)_1st.dv:	The first derivative of log(1/*R*)
log(1/*R*)_2nd.dv:	The second derivative of log(1/*R*).

Conflict of Interests

The authors declare that there is no conflict of interests regarding the publication of this paper.

Authors' Contribution

Qi Liu and Yilin Gu contributed equally to this paper.

Acknowledgments

This study was supported by the National Key Technologies Research and Development Program of China (2012BAD19BA04) and National Program on Key Basic Research Project (973 Program) (2013CB127700).

References

[1] Z. Q. Li and S. M. Zeng, *Wheat Rusts in China*, China Agriculture Press, Beijing, China, 2002.

[2] X. M. Chen, "Epidemiology and control of stripe rust on wheat," *Canadian Journal of Plant Pathology*, vol. 27, pp. 314–337, 2005.

[3] C. R. Wellings, "*Puccinia striiformis* in Australia: a review of the incursion, evolution, and adaptation of stripe rust in the period 1979–2006," *Australian Journal of Agricultural Research*, vol. 58, no. 6, pp. 567–575, 2007.

[4] X. Liu, C. Huang, Z. Sun, J. Liang, Y. Luo, and Z. Ma, "Analysis of population structure of *Puccinia striiformis* in Yunnan Province of China by using AFLP," *European Journal of Plant Pathology*, vol. 129, no. 1, pp. 43–55, 2011.

[5] C. Huang, Z. Sun, H. Wang, Y. Luo, and Z. Ma, "Effects of wheat cultivar mixtures on stripe rust: a meta-analysis on field trials," *Crop Protection*, vol. 33, pp. 52–58, 2012.

[6] A. M. Wan, Z. H. Zhao, X. M. Chen et al., "Wheat stripe rust epidemic and virulence of *Puccinia striiformis* f. sp. *Tritici* in China in 2002," *Plant Disease*, vol. 88, no. 8, pp. 896–904, 2004.

[7] J. F. Wang, C. Q. Chen, N. H. Lu et al., "SSR analysis of population genetic diversity of *Puccinia striiformis* f. sp. tritici in Sichuan Province, China," *Mycosystema*, vol. 29, pp. 206–213, 2010.

[8] J. M. Liang, Q. Wan, Y. Luo, and Z. H. Ma, "Population genetic structures of *Puccinia striiformis* in Ningxia and Gansu

provinces of China," *Plant Disease*, vol. 97, no. 4, pp. 501–509, 2013.

[9] S.-M. Zeng and Y. Luo, "Long-distance spread and interregional epidemics of wheat stripe rust in China," *Plant Disease*, vol. 90, no. 8, pp. 980–988, 2006.

[10] J. C. Zadoks, "Yellow rust on wheat studies in epidemiology and physiologic specialization," *Tijdschrift Over Plantenziekten*, vol. 67, no. 3, pp. 69–256, 1961.

[11] J. R. Burleigh, R. W. Romig, and A. P. Roelfs, "Characterization of wheat rust epidemics by number of uredia and urediniospores," *Phytopathology*, vol. 59, pp. 1229–1237, 1969.

[12] R. F. Line, "Stripe rust of wheat and barley in North America: a retrospective historical review," *Annual Review of Phytopathology*, vol. 40, pp. 75–118, 2002.

[13] S.-M. Zeng and Y. Luo, "Systems analysis of wheat stripe rust epidemics in China," *European Journal of Plant Pathology*, vol. 121, no. 4, pp. 425–438, 2008.

[14] H. Z. Wang, S. J. Li, Z. R. Huo, and J. A. Pang, "Physiological changes of cucumber after being infected by *Sphaerotheca fuliginea*," *Acta Agriculturae Boreali-Sinic*, vol. 21, no. 1, pp. 105–109, 2006.

[15] A. M. Wan, X. M. Chen, and Z. H. He, "Wheat stripe rust in China," *Australian Journal of Agricultural Research*, vol. 58, no. 6, pp. 605–619, 2007.

[16] W. Chen, C. Wellings, X. Chen, Z. Kang, and T. Liu, "Wheat stripe (yellow) rust caused by *Puccinia striiformis* f. sp. *tritici*," *Molecular Plant Pathology*, vol. 15, no. 5, pp. 433–446, 2014.

[17] R. L. Pu and P. Gong, *Hyperspectral Remote Sensing and Its Applications*, Higher Education Press, Beijing, China, 2000.

[18] J. S. West, C. Bravo, R. Oberti, D. Lemaire, D. Moshou, and H. A. McCartney, "The potential of optical canopy measurement for targeted control of field crop diseases," *Annual Review of Phytopathology*, vol. 41, pp. 593–614, 2003.

[19] T. Mewes, J. Franke, and G. Menz, "Spectral requirements on airborne hyperspectral remote sensing data for wheat disease detection," *Precision Agriculture*, vol. 12, no. 6, pp. 795–812, 2011.

[20] M. Y. Huang, W. J. Huang, L. Y. Liu et al., "Spectral reflectance feature of winter wheat single leaf infected with stripe rust and severity level inversion," *Transactions of the Chinese Society of Agriculture Engineering*, vol. 20, no. 1, pp. 176–180, 2004.

[21] H. An, H. G. Wang, R. Y. Liu, C. J. Cai, and Z. H. Ma, "Preliminary study on spectral characteristics of single leaf infected by *Puccinia striiformis*," *China Plant Protection*, vol. 25, no. 11, pp. 8–11, 2005.

[22] J. L. Zhao, L. S. Huang, W. J. Huang et al., "Hyperspectral measurements of severity of stripe rust on individual wheat leaves," *European Journal of Plant Pathology*, vol. 139, no. 2, pp. 401–411, 2014.

[23] D. Moshou, C. Bravo, J. West, S. Wahlen, A. McCartney, and H. Ramon, "Automatic detection of 'yellow rust' in wheat using reflectance measurements and neural networks," *Computers and Electronics in Agriculture*, vol. 44, no. 3, pp. 173–188, 2004.

[24] J.-B. Jiang, Y.-H. Chen, and W.-J. Huang, "Using hyperspectral derivative indices to diagnose severity of winter wheat stripe rust," *Optical Technique*, vol. 33, no. 4, pp. 620–623, 2007.

[25] J. C. Zhang, L. Yuan, R. L. Pu, R. W. Loraamm, G. J. Yang, and J. H. Wang, "Comparison between wavelet spectral features and conventional spectral features in detecting yellow rust for winter wheat," *Computers and Electronics in Agriculture*, vol. 100, pp. 79–87, 2014.

[26] L. Y. Liu, M. Y. Huang, W. J. Huang et al., "Monitoring stripe rust disease of winter wheat using multi-temporal hyperspectral airborne data," *Journal of Remote Sensing*, vol. 8, no. 3, pp. 275–281, 2004.

[27] W. J. Huang, D. W. Lamb, Z. Niu, Y. J. Zhang, L. Y. Liu, and J. Wang, "Identification of yellow rust in wheat using in-situ spectral reflectance measurements and airborne hyperspectral imaging," *Precision Agriculture*, vol. 8, no. 4-5, pp. 187–197, 2007.

[28] W. F. Leng, H. G. Wang, Y. Xu, and Z. H. Ma, "Preliminary study on monitoring wheat stripe rust with using UAV," *Acta Phytopathologica Sinica*, vol. 42, no. 2, pp. 202–205, 2012.

[29] L. Y. Liu, X. Y. Song, C. J. Li, L. Qi, W. J. Huang, and J. H. Wang, "Monitoring and evaluation of the diseases of and yield winter wheat from multi-temporal remotely-sensed data," *Transactions of the Chinese Society of Agricultural Engineering*, vol. 25, no. 1, pp. 137–143, 2009.

[30] J. B. Guo, C. Huang, H. G. Wang, and Z. H. Ma, "Preliminary study on remote sensing monitoring wheat stripe rust based on SPOT5 image," *Acta Phytophylacica Sinica*, vol. 36, no. 5, pp. 473–474, 2009.

[31] S. Dutta, S. K. Singh, and M. Khullar, "A case study on forewarning of yellow rust affected areas on wheat crop using satellite data," *Journal of the Indian Society of Remote Sensing*, vol. 42, no. 2, pp. 335–342, 2014.

[32] D. M. Gates, H. J. Keegan, J. C. Schleter, and V. R. Weidner, "Spectral properties of plants," *Applied Optics*, vol. 4, no. 1, pp. 11–20, 1965.

[33] E. B. Knipling, "Physical and physiological basis for the reflectance of visible and near-infrared radiation from vegetation," *Remote Sensing of Environment*, vol. 1, no. 3, pp. 155–159, 1970.

[34] H. W. Gausman, "Leaf reflectance of near-infrared," *Photogrammetric Engineering*, vol. 40, no. 2, pp. 183–191, 1974.

[35] H. W. Gausman, W. A. Allen, R. Cardenas, and A. J. Richardson, "Relation of light reflectance to histological and physical evaluations of cotton leaf maturity," *Applied Optics*, vol. 9, no. 3, pp. 545–552, 1970.

[36] H. W. Gausman, W. A. Allen, and D. E. Escobar, "Refractive index of plant cell walls," *Applied Optics*, vol. 13, no. 1, pp. 109–111, 1974.

[37] R. D. Jackson, "Remote sensing of biotic and abiotic plant stress," *Annual Review of Phytopathology*, vol. 24, no. 1, pp. 265–287, 1986.

[38] T. H. Demetriades-Shah, M. D. Steven, and J. A. Clark, "High resolution derivative spectra in remote sensing," *Remote Sensing of Environment*, vol. 33, no. 1, pp. 55–64, 1990.

[39] J. H. Wang, C. J. Zhao, and W. J. Huang, *The Application of Agricultural Quantitative Remote Sensing*, Science Press, Beijing, China, 2008.

[40] B. J. Yoder and R. E. Pettigrew-Crosby, "Predicting nitrogen and chlorophyll content and concentrations from reflectance spectra (400–2500 nm) at leaf and canopy scales," *Remote Sensing of Environment*, vol. 53, no. 3, pp. 199–211, 1995.

[41] V. C. LaCapra, J. M. Melack, M. Gastil, and D. Valeriano, "Remote sensing of foliar chemistry of inundated rice with imaging spectrometry," *Remote Sensing of Environment*, vol. 55, no. 1, pp. 50–58, 1996.

[42] Y. L. Grossman, S. L. Ustin, S. Jacquemoud, E. W. Sanderson, G. Schmuck, and J. Verdebout, "Critique of stepwise multiple linear regression for the extraction of leaf biochemistry information from leaf reflectance data," *Remote Sensing of Environment*, vol. 56, no. 3, pp. 182–193, 1996.

[43] G. A. Blackburn, "Spectral indices for estimating photosynthetic pigment concentrations: a test using senescent tree leaves," *International Journal of Remote Sensing*, vol. 19, no. 4, pp. 657–675, 1998.

[44] L. Serrano, J. Peñuelas, and S. L. Ustin, "Remote sensing of nitrogen and lignin in Mediterranean vegetation from AVIRIS data: decomposing biochemical from structural signals," *Remote Sensing of Environment*, vol. 81, no. 2-3, pp. 355–364, 2002.

[45] Y. Hao, X. D. Sun, R. J. Gao, Y. Pan, and Y. Liu, "Application of visible and near infrared spectroscopy to identification of navel orange varieties using SIMCA and PLS-DA methods," *Transactions of the Chinese Society of Agricultural Engineering*, vol. 26, no. 12, pp. 373–377, 2010.

[46] H. Qin, H.-R. Wang, W.-J. Li, and X.-X. Jin, "Application of DPLS-based LDA in corn qualitative near infrared spectroscopy analysis," *Spectroscopy and Spectral Analysis*, vol. 31, no. 7, pp. 1777–1781, 2011.

[47] M. Y. Huang, J. H. Wang, W. J. Huang, Y. D. Huang, C. J. Zhao, and A. M. Wan, "Hyperspectral character of stripe rust on winter wheat and monitoring by remote sensing," *Transactions of the CSAE*, vol. 19, no. 6, pp. 154–158, 2003.

[48] K.-L. Tan, Y.-Q. Wan, Y.-D. Yang, and Q.-B. Duan, "Study of hyperspectral remote sensing for archaeology," *Journal of Infrared and Millimeter Waves*, vol. 24, no. 6, pp. 437–440, 2005.